Novel 3D ultrasound image-based biomarkers based on a feature selection from a 2D standardized vessel wall thickness map: a tool for sensitive assessment of therapies for carotid atherosclerosis

2013 Phys. Med. Biol. 58 5959

(http://iopscience.iop.org/0031-9155/58/17/5959)

IOP Publishing Physics in Medicine and Biology

Phys. Med. Biol. **58** (2013) 5959–5982 doi:10.1088/0031-9155/58/17/5959

Novel 3D ultrasound image-based biomarkers based on a feature selection from a 2D standardized vessel wall thickness map: a tool for sensitive assessment of therapies for carotid atherosclerosis

Bernard Chiu, Bing Li and Tommy W S Chow

Department of Electronic Engineering, City University of Hong Kong, Hong Kong

E-mail: bcychiu@cityu.edu.hk, bingli5@student.cityu.edu.hk and eetchow@cityu.edu.hk

Received 28 March 2013, in final form 25 June 2013
Published 12 August 2013
Online at stacks.iop.org/PMB/58/5959

Abstract

With the advent of new therapies and management strategies for carotid atherosclerosis, there is a parallel need for measurement tools or biomarkers to evaluate the efficacy of these new strategies. 3D ultrasound has been shown to provide reproducible measurements of plaque area/volume and vessel wall volume. However, since carotid atherosclerosis is a focal disease that predominantly occurs at bifurcations, biomarkers based on *local* plaque change may be more sensitive than global volumetric measurements in demonstrating efficacy of new therapies. The ultimate goal of this paper is to develop a biomarker that is based on the *local* distribution of vessel-wall-plus-plaque thickness change (*VWT-Change*) that has occurred during the course of a clinical study. To allow comparison between different treatment groups, the *VWT-Change* distribution of each subject must first be mapped to a standardized domain. In this study, we developed a technique to map the 3D *VWT-Change* distribution to a 2D standardized template. We then applied a feature selection technique to identify regions on the 2D standardized map on which subjects in different treatment groups exhibit greater difference in *VWT-Change*. The proposed algorithm was applied to analyse the *VWT-Change* of 20 subjects in a placebo-controlled study of the effect of atorvastatin (Lipitor). The average *VWT-Change* for each subject was computed (i) over all points in the 2D map and (ii) over feature points only. For the average computed over all points, 97 subjects per group would be required to detect an effect size of 25% that of atorvastatin in a six-month study. The sample size is reduced to 25 subjects if the average were computed over feature points only. The introduction of this sensitive quantification technique for carotid atherosclerosis progression/regression would allow many proof-of-principle studies to be

performed before a more costly and longer study involving a larger population is held to confirm the treatment efficacy.

(Some figures may appear in colour only in the online journal)

1. Introduction

Stroke is among the leading causes of death and disability worldwide, with estimated direct and indirect costs in 2010 of $73.7 billion in the United States alone (Lloyd-Jones *et al* 2010). However, stroke has a larger impact in developing countries such as China, which has a morality rate of stroke that is more than seven times higher than that in the United States in the population group aged 40–64 (He *et al* 2005). A major portion of strokes is ischemic, mostly caused by the blockage of a cerebral artery by a thrombotic embolus. Carotid atherosclerosis is a major cause of thrombosis and subsequent cerebral emboli (Eicke *et al* 1995, Golledge *et al* 2000). Nonetheless, most strokes associated with carotid atherosclerosis can be prevented by lifesytle/dietary changes, medical and surgical treatments (Gorelick 1994, Spence 2007). These treatment strategies are required to be validated in clinical trials. Traditional clinical trials use incidence of vascular events, stenosis (NASCET Steering Committee 1991, ECST Collaborative Group 1995) and intima-media thickness (IMT) (O'Leary and Polak 2002) to evaluate the severity of carotid disease. These trials must be very large in order to demonstrate the effects of different treatments in a statistically significant way. Therefore, parallel to the development of new therapies, an equally important requirement is the development of treatment-specific measurement tools or biomarkers for evaluation of carotid atherosclerosis and serial monitoring of disease progression or regression. Sensitive, non-invasive 3D imaging technique allowing plaque visualization and quantification will play a vital role in the development of such biomarker.

The ability of 3D ultrasound for direct quantification of carotid plaque, such as total plaque area/volume (Spence *et al* 2002, Landry *et al* 2004, Ainsworth *et al* 2005) and vessel wall volume (VWV) (Egger *et al* 2007), has been established. By virtue of the additional dimensions, these measures are more sensitive to disease progression/regression than IMT (Ainsworth *et al* 2005, Pollex *et al* 2005). However, plaque dimension alone, although serving as direct measurements on plaque change, could not identify local change of plaque. The knowledge of local plaque change will allow for more sensitive tests to be performed, making the size of a clinical trial smaller and the duration shorter. In addition, carotid atherosclerosis is a focal disease, predominantly occurs at the bifurcations. Sudden focal progression is associated with an elevated risk of vascular events (Spence *et al* 2002, Hirano *et al* 2011). Therefore, if the regional distribution of plaque change could be visualized and quantified, the risk of vascular events can be monitored more effectively. To quantify the 3D distribution of plaque change, we have developed a metric to quantify the vessel-wall-plus-plaque-thickness change (*VWT-Change*) on a point-by-point basis, resulting in a 3D map showing distribution of *VWT-Change* (Chiu *et al* 2008b).

Although the 3D *VWT-Change* maps provide rich information regarding the 3D distribution of vessel wall and plaque progression and regression, there are hundreds if not thousands points on each 3D *VWT-Change* map and it is very difficult to interpret these overwhelming data and make clinical conclusions. Thus, the ultimate goal of this paper is to develop a sensitive biomarker that can summarize the information provided in the 3D *VWT-Change* maps. The major application of this biomarker will be on evaluating the effects of different types of plaque stabilization strategies. This biomarker will be validated by

determining the sample sizes needed to detect statistically significant effects of an intensive atorvastatin therapy. Since the arterial geometry is highly variable between subjects, there is a need to map 3D *VWT-Change* maps to a standardized template so that correspondence points in different carotid arteries are mapped to the same position in the standardized template to facilitate localized comparison. Considering the fact that visualization and interpretation of the 3D map is unnecessarily difficult due to the complex topology of the carotid artery at the bifurcation, a 2D standardized map is preferred. We have previously developed a mapping technique to cut and unfold a 3D carotid surface so that the 3D *VWT-Change* distribution can be visualized in a 2D view (Chiu *et al* 2008a). This algorithm has been used in clinical studies investigating the temporal and spatial changes of VWT when subjects were treated using different strategies (Egger *et al* 2008, Krasinski *et al* 2009), in an interscan reproducibility evaluation (Egger *et al* 2008) and in an experimental study involving luminal ulceration and fissure detection (Chiu *et al* 2009). However, our 2D mapping approach has a major disadvantage. The 2D maps produced for different subjects have different shapes (e.g., see figure 4 in Egger *et al* (2008)). Many other conformal (angle-preserving) or area-preserving techniques developed to flatten tubular surfaces also suffer from the same problem (Bartroli *et al* 2001, Haker *et al* 2000, Zhu *et al* 2005). Thus, 2D VWT maps generated for the same subject at different time points or *VWT-Change* maps generated for different subjects must be matched visually before regional comparisons of the maps can be performed. However, visual matching of 2D maps is subjective and prone to operator variability.

Thus, there are two major goals in this paper. The first goal is to develop a novel technique that transforms the 3D *VWT-Change* maps into a 2D standardized map to allow for quantitative and localized assessment of vessel wall and plaque progression and regression. The second goal is to develop sensitive biomarkers based on the *VWT-Change* distribution on the 2D *VWT-Change* maps. To design sensitive biomarkers that can detect the effect of plaque stabilization strategies, we first applied a feature selection technique to identify regions on the standardized 2D map on which subjects in different treatment groups demonstrate greater difference in *VWT-Change*. A mutual-information-based feature selection technique was applied for this purpose (Chow and Huang 2005). Mutual information was chosen as the criteria to evaluate the discriminating ability of a subset of features because it is less affected by noise (Battiti 1994). Since the selected regions exhibit greater plaque response difference between treatment groups, we hypothesize that it would require fewer subjects to show statistical significant difference in a biomarker that only accounts for the *VWT-Change* values on these regions. In this paper, we will compare average *VWT-Change* for each subject in two settings, in which averages are computed (i) over all points and (ii) selected points in the 2D *VWT-Change* maps. Statistical tests are then used to evaluate whether the average computed in setting (ii) is more sensitive to the treatment effect than that computed in setting (i).

2. Methods

2.1. Subjects

We demonstrate the application of the proposed algorithm using 3D ultrasound carotid images of two groups of subjects with ten in each group. These subjects participated in a clinical study focusing on evaluating the effect of atorvastatin (Ainsworth *et al* 2005). They were asymptomatic with carotid stenosis >60% (according to carotid Doppler flow velocities). 3D ultrasound images of these subjects were acquired at baseline and three months later. Subjects were allocated in a double-blind fashion to identical placebo or 80 mg atorvastatin tablets (Lipitor). All subjects were recruited from The Premature Atherosclerosis Clinic

and The Stroke Prevention Clinic at University Hospital (London Health Sciences Centre, London, Canada) and the Stroke Prevention and Atherosclerosis Research Centre (Robarts Research Institute, London, Canada). All subjects provided written informed consent to the study protocol, which was approved by The University of Western Ontario Standing Board of Human Research Ethics.

2.2. Acquisition of 3D ultrasound carotid images

The 3D carotid ultrasound system has been described in detail elsewhere (Fenster *et al* 2001) and is summarized here. Briefly, the 3D ultrasound images were acquired by translating an ultrasound transducer (L12-5, Philips, Bothel, WA) with a custom-made mechanical assembly along the neck of the subject for approximately 4.0 cm at a uniform speed of 3 mm s^{-1}. The 2D ultrasound frames acquired using the ultrasound machine (ATL HDI 5000, Philips, Bothel, WA) were digitized at 30 Hz and reconstructed into a 3D image. A sonographer would then examine the acquired 3D image to ensure that the bifurcation was located at the approximate centre of the image volume. The voxel size of the 3D ultrasound images were approximately $0.1 \times 0.1 \times 0.15$ mm^3.

2.3. Construction of 3D vessel-wall-plus-plaque thickness change map

The algorithm for constructing the 3D *VWT-Change* map has been described elsewhere (Chiu *et al* 2008b). In the following subsections, we will briefly summarize the algorithm.

2.3.1. Arterial wall/lumen segmentation and surface reconstruction. First, the outer wall and the lumen boundary of the carotid artery were required to be segmented. Because the images involved in this study have been segmented in a previous study for VWV quantification (Krasinski *et al* 2009) and because of the fact that manual segmentation has been considered most reliable and used as ground truth to evaluate semiautomatic contours (Ukwatta *et al* 2011), the manually segmented contours were used in this study. These contours were segmented by a single observer blinded to subject identity, treatment and time point. The carotid bifurcation was first located from the 3D ultrasound image. An axis was placed parallel with the longitudinal axis of the common carotid artery (CCA) and centred at the bifurcation. The 3D image was then resliced perpendicular with the longitudinal axis at an interslice distance of 1 mm. The outer wall and the lumen boundaries of the common, internal and external carotid arteries (CCA, ICA and ECA respectively) were segmented on each resliced 2D transverse plane, resulting in a stack of 2D contours. Adjacent 2D contours are then matched using the modified symmetric correspondence algorithm (Chiu *et al* 2008b) to construct the outer wall surface and lumen surface for each subject.

2.3.2. Computation of the VWT and VWT-Change map. The point-by-point VWT of the carotid artery acquired at baseline was obtained on a slice-by-slice basis by using the modified symmetric correspondence algorithm and superimposed on the outer wall contour (Chiu *et al* 2008b). To allow direct comparison, the outer wall surface obtained at the follow-up scanning session was registered with that obtained for the first time point using the modified iterative closest point algorithm we developed (Chiu *et al* 2012). The transformation thus obtained was also applied on the lumen surface acquired at follow-up in order to align with the registered wall surface. Point-by-point VWT at follow-up was computed on the same transverse slice as was computed at baseline and superimposed on the outer wall surface. The outer wall surfaces obtained at baseline and follow-up were matched according to the angular positions. For each

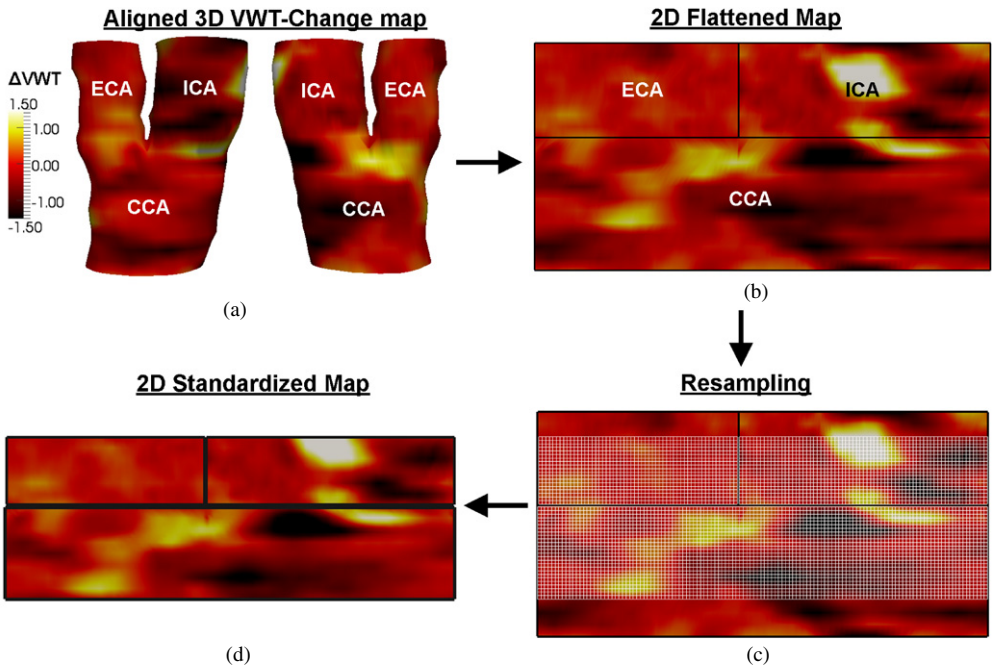

Figure 1. Schematic diagram of the 2D standardized map construction algorithm.

pair of corresponding points, the *VWT-Change* was computed, colour-coded and superimposed on the arterial wall surface (e.g., figures 5(g) and (h)), which we refer to as *VWT-Change* map hereafter.

2.4. Construction of the 2D standardized map

A simplified version of this 2D standardized mapping technique has been introduced in Chiu *et al* (2013), in which 2D maps were generated for CCA only. The technique described in this paper was designed to generate 2D standardized maps for ICA and ECA in addition to CCA. The flowchart of the algorithm used to construct the 2D standardized map is shown in figure 1. The algorithm consists of three steps: (1) the 3D *VWT-Change* map was aligned with the standard local coordinate frame; (2) the aligned 3D map was mapped to a 2D rectangular domain; (3) the 2D rectangular map was resampled to obtain the 2D standardized map. Each step is individually described in the following sections.

2.4.1. Alignment of 3D VWT-Change map. A longitudinal axis was defined before segmenting each artery. Before constructing a 2D standardized map, the longitudinal axis of each artery was aligned with the z-axis of a local coordinate frame with the positive z-axis pointing to the downstream direction. The bifurcation of each wall surface, as defined using our technique described in Chiu *et al* (2008b), was moved to the origin of the local coordinate frame. The centroids of the ECA and ICA contours immediately distal to the bifurcation were computed and denoted as C_{ECA} and C_{ICA}. The vector pointing from C_{ECA} to C_{ICA} was aligned with the x-axis (figure 2(b)). $\hat{x}$, $\hat{y}$ and $\hat{z}$ are used to denote the unit vectors of x-, y- and z-axis respectively hereafter.

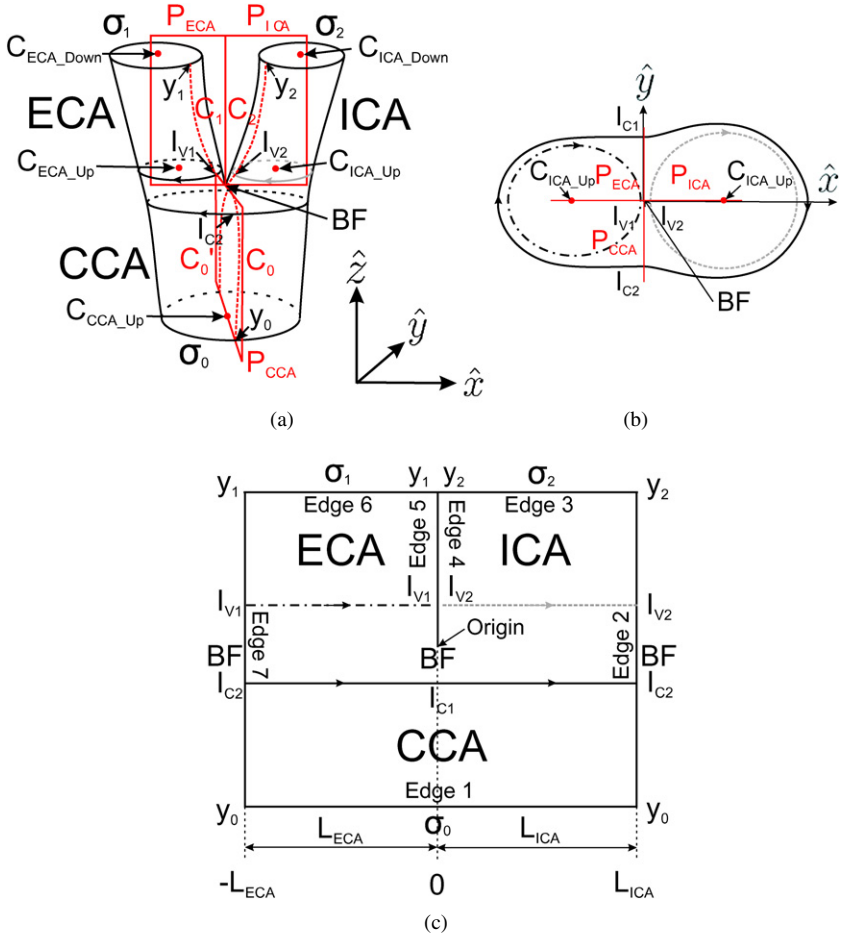

Figure 2. (a) Schematic diagram of the carotid arteries with the three planes, P_{ICA}, P_{ECA} and P_{CCA}, cutting the internal, external and common carotid arteries (ICA, ECA and CCA), respectively. The labels on the diagram were all defined in section 2.4. (b) The cross-section of the carotid arteries showing the contours at ICA, ECA and CCA that are closest to the bifurcation (BF) (c) The 2D standardized map.

2.4.2. 2D flattened map generation. The aligned 3D map of each artery was then cut, unfolded and mapped to a rectangular domain with the bifurcation at the origin (figures 1(b) and 2(c)). The orientation of the planes cutting CCA, ICA and ECA were defined by a line and a vector lying on it as follows (figure 2(a)).

- The plane cutting the CCA is labelled as P_{CCA} in figure 2(a), which was defined by (i) the line connecting the centroid of the CCA contour most distal to the bifurcation, $C_{\mathrm{CCA_{UP}}}$, and the bifurcation apex, BF and (ii) the $\hat{y}$ vector.
- The planes cutting the ICA and ECA are labelled as P_{ICA} and P_{ECA} in figure 2(a) respectively, which were defined by (i) the line connecting the centroid of the contour immediately distal to the bifurcation, $C_{\mathrm{ICA_{UP}}}$ (or $C_{\mathrm{ECA_{UP}}}$), and the centroid of the contour farthest away from the bifurcation, $C_{\mathrm{ICA_{Down}}}$ (or $C_{\mathrm{ECA_{Down}}}$) and (ii) the $\hat{x}$ vector.

The intersecting lines between the cutting planes and the CCA, ECA and ICA are shown as red dotted lines and labelled C_0, C_1 and C_2 respectively. The arterial surface was unfolded

to a rectangular domain shown in figure 2(c). The 3D carotid surface has three boundary components, which are labelled as σ_0, σ_1 and σ_2. The intersecting lines between the planes P_{CCA}, P_{ECA} and P_{ICA} and the carotid surface were denoted by C_0, C_1 and C_2 respectively. C_0, C_1 and C_2 run from σ_0, σ_1 and σ_2 respectively and meets at the bifurcation apex. The boundary of the 3D carotid surface after being cut was defined by the original boundaries σ_0, σ_1 and σ_2 and the intersecting lines C_0, C_1 and C_2. These boundaries were mapped to seven straight edges in the rectangular domain. The corresponding 3D locations of edges 1–7 labelled in figure 2(c) are listed below.

Edge 1 $y_0 \xrightarrow{\sigma_0} y_0$
Edge 2 $y_0 \xrightarrow{C_0} \mathrm{BF} \xrightarrow{C_2} y_2$
Edge 3 $y_2 \xrightarrow{\sigma_2} y_2$
Edge 4 $y_2 \xrightarrow{C_2} \mathrm{BF}$
Edge 5 $\mathrm{BF} \xrightarrow{C_1} y_1$
Edge 6 $y_1 \xrightarrow{\sigma_1} y_1$
Edge 7 $y_1 \xrightarrow{C_1} \mathrm{BF} \xrightarrow{C_0} y_0$

The CCA, ICA and ECA transverse contours were mapped to the standardized rectangular domain in the following way. The plane P_{CCA} cuts the CCA along C_0 on the negative y side of the 3D coordinate frame and C_0' on the positive y side (figure 2(a)). Figure 2(b) shows a transverse CCA contour in the cross-sectional view. The CCA contour intersects with C_0 at I_{C2} and C_0' at I_{C1}. The arc-length of the contour segment from I_{C2} to I_{C1} was scaled and mapped in the clockwise direction to a straight line from $x = -L_{\mathrm{ECA}}$ to 0 in the 2D standardized map as shown in figure 2(c). The segment from I_{C1} to I_{C2} was mapped to a straight line from $x = 0$ to $x = L_{\mathrm{ICA}}$ in the same way. The ECA and ICA contours intersects C_1 and C_2 at I_{V1} and I_{V2} respectively. The ECA contour starting and ending at I_{V1} was mapped in a clockwise direction to a straight line starting at $x = -L_{\mathrm{ECA}}$ and ending at $x = 0$. Similarly, the ICA contour starting and ending at I_{V2} was mapped to a straight line starting at $x = 0$ and ending at $x = L_{\mathrm{ICA}}$. The last thing remains to be considered is the dimension of the standardized map. Each 3D map was cut by P_{CCA}, dividing the 3D surface into the ECA and ICA sides (figure 3). By dividing the ECA surface area by the height of the 3D surface, we obtained the horizontal length of ECA on the 2D map, which we denote as $L_{\mathrm{ECA},i}$ for the ith artery. L_{ECA} was computed by taking the average of $L_{\mathrm{ECA},i}$ for all arteries. L_{ICA} was computed in the same way.

2.4.3. Resampling. The 2D flattened map of each artery was then sampled in a 0.3 mm interval on both the horizontal and vertical directions (figure 1(c)). The axial, lateral and elevational resolutions of the L12-5 transducer are approximately 0.6, 0.6 and 2 mm at 4 cm penetration depth (Browne *et al* 2004). We made a conservative choice of 0.3 mm sampling interval to make sure that plaques would not be missed. Resampling was performed to construct a 2D standardized map so that quantitative comparisons of *VWT-Change* distribution of all arteries can be performed on a point-by-point basis. Furthermore, the resampled *VWT-Change* distribution can be interpreted as a set of features in a feature selection analysis, which is the focus of the following section. In our study, because the longitudinal coverage of different 3D carotid ultrasound images may be different, the length of the artery on which segmentation can be performed may be different. Since the 2D standardized maps of all arteries must be the same, resampling was only performed in the region where all 2D flattened maps overlap, which may be significantly smaller than the 2D flattened map for some arteries, such as the artery shown in figure 1(c). The resampled 2D map in figure 1(d) is referred to as the 2D standardized map hereafter and used in the following feature selection analysis.

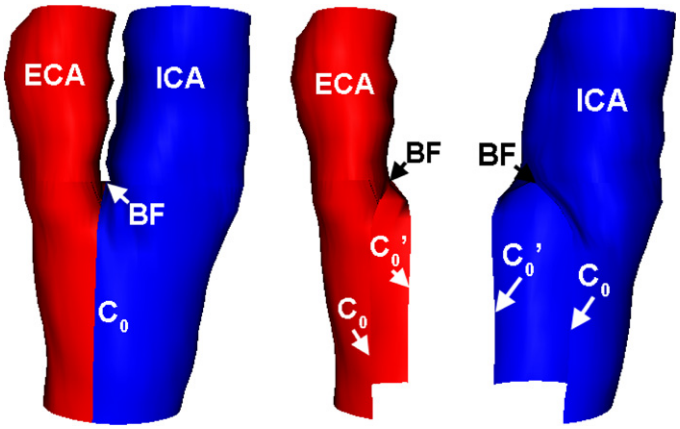

Figure 3. For calculation of the two parameters, L_{ECA} and L_{ICA}, required in the 2D standardized map construction (section 2.4), each carotid surface was cut into the ECA (red) and ICA (blue) sides by P_{CCA} as shown in (a). (b) and (c) Show the ECA and ICA sides respectively with C_0 and C_0' labelled, which are the intersection lines between the carotid surface and P_{CCA}. BF denotes the bifurcation.

2.5. Feature selection

Given a number of subjects belonging to different treatment groups, feature selection analysis identifies a subset of *VWT-Change* values on the standardized map that are most correlated with which treatment group an artery belongs to. This technique helps us to locate the regions where there are significant differences between the atorvastatin and the placebo group. The feature selection algorithm applied in this paper was based on mutual information and was described in Chow and Huang (2005). The algorithm is supervised, meaning that the information on whether a subject belongs to the placebo or the atorvastatin group was provided as an input to the algorithm. Briefly, mutual information is a quantity that quantifies the correlation between random variables. Suppose knowing the *VWT-Change* value at position x_m of the standardized map, denoted as f_m, reduces much uncertainty regarding which treatment group, C, an artery belongs to (which is either the atorvastatin or placebo group in our study), the mutual information $I(f_m; C)$ is high.

The flow chart of the algorithm is shown in figure 4. Briefly, F represents the candidate feature set and S represents the selected feature set. F was initialized to contain all the features (i.e., *VWT-Change* values at all points in a standardized map) and S was initialized to be an empty set. The feature selection algorithm selects a feature, f_m, at each iteration that maximizes $I(S + f_m; C)$, which is the mutual information between the feature set $S + f_m$ and the treatment group C. $S + f_m$ was formed by adding $f_m \in F$ to the existing feature set S, which contains all features selected in previous iterations. The termination criterion was defined based on the P-value of the t-test performed for a metric denoted as $\overline{\Delta VWT}_S$ between the placebo and atorvastatin group. This metric will be defined in equation (5*b*) and described in section 2.6.2.

In the original algorithm, if f_m represents redundant information that is similar to a feature in S, f_m was not included in S even though adding this feature would maximize $I(S + f_m; C)$. The purpose of excluding points that represent redundant information was to reduce the computation complexity of classification processes. However, *VWT-Change* measurements in a neighbourhood are usually continuous and therefore the *VWT-Change* measurements associated with neighbouring points may carry similar information in the classification

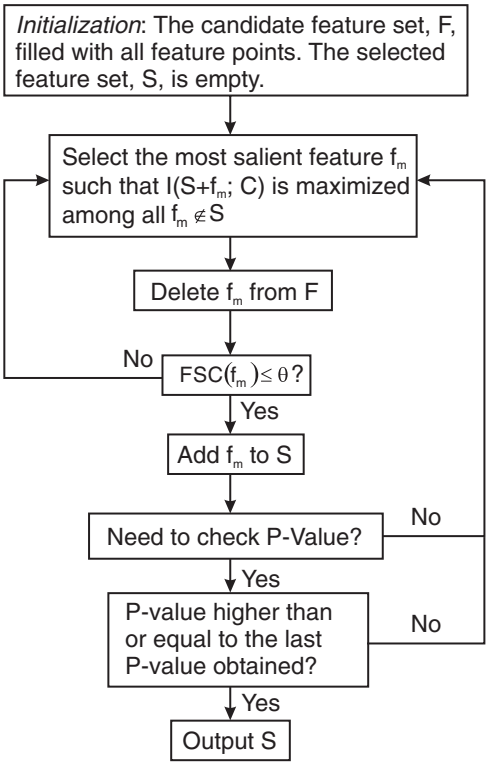

Figure 4. Flow chart of the mutual-information-based feature selection algorithm. *P*-value shown in the flow chart denotes the *P*-value resulting from a *t*-test between the placebo and atorvastatin group based on $\overline{\Delta VWT}_S$. This *P*-value was checked starting at the time when 10% of the total number of feature points have been selected, and was checked at a 1% increment thereafter. Also note that in this application the redundancy check step (i.e., $\mathrm{FSC}(f_m) \leqslant \theta$?) was bypassed by setting $\theta = 1$.

point-of-view. Yet, for our purposes, the whole region on which different treatment groups exhibit different *VWT-Change* distribution should be included. The similarity between f_m and the features already included in S is quantified by a feature similarity coefficient (FSC), which was defined by:

$$\mathrm{FSC}(f_m) = \arg\max_{f_i \in S} \left(\frac{I(f_m; f_i)}{H(f_i)} \right) \tag{1}$$

where $H(\cdot)$ is the entropy.

The original algorithm adds the feature f_m only if $\mathrm{FSC}(f_m) \leqslant \theta$. As $H(f_i) = H(f_i|f_m) + I(f_i; f_m) \geqslant I(f_i; f_m)$, $\mathrm{FSC}(f_m) \leqslant 1$. To bypass the redundancy check, θ was set to be 1 in our application. This ensured that features were selected only based on how it correlates with the identity of the treatment group.

2.6. Statistical tests

2.6.1. Point-by-point group analysis of VWT-Change. Since the 3D VWT and *VWT-Change* maps were all mapped to the 2D standardized map, point-by-point group averages of VWT and *VWT-Change* can be computed and displayed. The 2D standardized map with the average

VWT and *VWT-Change* computed for the placebo and atorvastatin groups will be shown in section 3.2.

Another application of the 2D standardized map is to identify subjects that are associated with rapid focal progression and regression of VWT. Krasinski *et al* (2009) identified that the placebo group was associated with VWV progression, whereas the atorvastatin group was associated with VWV regression. In this part, we identify, at each point, the subject with the maximum VWT progression among the ten placebo subjects, and the subject with maximum VWT regression among the ten subjects treated by atorvastatin. This information was plotted on the 2D standardized map, which shows the distribution regarding which subject was associated with the maximum progression/regression at each point. The procedure is summarized below.

(i) Each point at the 2D map (denoted as p_i) of each subject is associated with a *VWT-Change* value. For the placebo group, at each p_i, the maximum *VWT-Change* among the ten subjects, $\mathrm{Max}\Delta VWT(p_i)$, were obtained (equation (2*a*)). For the group treated by atorvastatin, the minimum *VWT-Change* (i.e., maximum regression of *VWT*) among the ten subjects, $\mathrm{Min}\Delta VWT(p_i)$, were obtained:

$$\mathrm{Max}\Delta VWT(p_i) = \max\{\Delta VWT_j(p_i)\}_{j=1}^{10} \tag{2a}$$

$$\mathrm{Min}\Delta VWT(p_i) = \min\{\Delta VWT_j(p_i)\}_{j=1}^{10} \tag{2b}$$

where $\Delta VWT_j(p_i)$ is *VWT-Change* of Subject j at p_i.

(ii) In order to display the subject with the greatest increase and greatest decrease of VWT on a point-by-point basis on the 2D standardized map for the placebo and the atorvastatin groups respectively, two quantities were defined as follows:

$$SubjectIndex_P(p_i) = \begin{cases} \arg\max_j \{\Delta VWT_j(p_i)\}_{j=1}^{10}, & \mathrm{Max}\Delta VWT(p_i) > 1\mathrm{mm} \\ -3, & \text{otherwise} \end{cases} \tag{3a}$$

$$SubjectIndex_A(p_i) = \begin{cases} \arg\min_j \{\Delta VWT_j(p_i)\}_{j=1}^{10}, & \mathrm{Min}\Delta VWT(p_i) < -1\mathrm{mm} \\ -3, & \text{otherwise.} \end{cases} \tag{3b}$$

Equation (3*a*) sets $SubjectIndex_P(p_i)$ to be the identification number (from 1 to 10) of the placebo subject with the maximum ΔVWT at point p_i, if $\mathrm{Max}\Delta VWT(p_i) > 1$ mm. Equation (3*b*) sets $SubjectIndex_A(p_i)$ to be the identification number (from 1 to 10) of the atorvastatin subject with the minimum ΔVWT (i.e., maximum VWT regression) at point p_i, if $\mathrm{Min}\Delta VWT(p_i) < -1$ mm. Since the purpose was to find out subjects with rapid focal progression or regression, identification numbers of subjects were only plotted when the maximum VWT progression or regression is greater than 1 mm. (Figures 8(a) and (e)). -3 was chosen to represent regions with progression and regression smaller than 1 mm as it is well separated and easily distinguished from valid subject identification numbers (1 to 10) when $SubjectIndex_P$ or $SubjectIndex_A$ is colour-coded and displayed as 2D maps.

If a placebo subject j has a large area where its ΔVWT is maximum among the ten subjects (i.e., there is a large area with $SubjectIndex_P(p_i) = j$), this subject would be flagged and their VWT and *VWT-Change* maps studied by physicians, who would then determine whether intervention is necessary to mitigate the elevated risk of vascular events. Similarly, an atorvastatin subject j with large area on the 2D standardized map where $SubjectIndex_A(p_i) = j$ can also be identified. Physicians can study the medical profiles of this subject and investigate which factors contribute to the larger VWT regression compared to other subjects in the group.

2.6.2. T-tests on average VWT-Change computed over different regions. We hypothesized that a biomarker computed over the region selected by the feature selection technique is more sensitive than its correspondence computed over the entire *VWT-Change* map. In this section, we compare the average *VWT-Change* for each artery computed over three different regions: (a) all points in the 2D *VWT-Change* map, (b) S, the set containing all points selected by the feature selection technique and (c) $F_{\mathrm{GD}>0}$, which is defined in the following two paragraphs. T-tests were performed for these averages. Each t-test is associated with a P-value, which reflects the sensitivity of these averages in evaluating the statistical difference between the atorvastatin and placebo groups. As described in section 2.5 and shown in figure 4, the termination criterion of the feature selection algorithm is based on the P-value of one of the t-tests described here. The detail regarding the stopping criterion will be described after defining how the three averages were obtained.

For each point p_i on the standardized map, a metric denoted as $\mathrm{GD}\Delta VWT(p_i)$, was defined to describe the difference between average *VWT-Change* of the placebo group, $\overline{\Delta VWT_P}(p_i)$, and the atorvastatin group, $\overline{\Delta VWT_S}(p_i)$:

$$\mathrm{GD}\Delta VWT(p_i) = \overline{\Delta VWT_P}(p_i) - \overline{\Delta VWT_S}(p_i) \tag{4}$$

where $\overline{\Delta VWT_P}(p_i) = \frac{1}{10}\sum_{j=1}^{10} \Delta VWT_j(p_i)$ and $\overline{\Delta VWT_S}(p_i) = \frac{1}{10}\sum_{j=11}^{20} \Delta VWT_j(p_i)$, in which subjects on placebo were indexed from 1 to 10 and those on atorvastatin were indexed from 11 to 20.

Since it is expected that VWT for the atorvastatin group would decrease more than for the placebo group, $\mathrm{GD}\Delta VWT(p_i)$ is expected to be positive. We classified the points identified by the feature selection algorithm into two groups. The subset of feature points with $\mathrm{GD}\Delta VWT(p_i) > 0$ and $\mathrm{GD}\Delta VWT(p_i) \leqslant 0$ are respectively denoted by $F_{\mathrm{GD}>0}$ and $F_{\mathrm{GD}\leqslant 0}$.

For each artery, we defined the following three averages, which are the average *VWT-Change* computed over (a) A, the set containing all points in the 2D *VWT-Change* map, (b) S and (c) $F_{\mathrm{GD}>0}$:

$$\overline{\Delta VWT_j} = \frac{1}{\#A}\sum_{p_i \in A} \Delta VWT_j(p_i) \tag{5a}$$

$$\overline{\Delta VWT}_{S,j} = \frac{1}{\#S}\sum_{p_i \in S} \Delta VWT_j(p_i) \tag{5b}$$

$$\overline{\Delta VWT}_{F_{\mathrm{GD}>0,j}} = \frac{1}{\#F_{\mathrm{GD}>0}}\sum_{p_i \in F_{\mathrm{GD}>0}} \Delta VWT_j(p_i) \tag{5c}$$

where the subscript j indicates the metrics are computed for subject j. When statistical tests were performed for these three metrics, averages of equations (5*a*)–(5*c*) were computed for the whole placebo or atorvastatin group. These averages are denoted as in equations (5*a*)–(5*c*) but with the subscript j dropped.

T-tests were performed for the three metrics above and the associated P-values were obtained. We hypothesize that the metrics that account for the ΔVWT values at selected feature points are more sensitive in detecting the statistical difference between the atorvastatin and placebo groups than $\overline{\Delta VWT}$, which is a scaled version of VWV. Sample size estimates for the three metrics were also computed by using the following equation:

$$n = \frac{(z_{\alpha/2} + z_{\beta})^2\left(\sigma_P^2 + \sigma_S^2\right)}{\delta^2} \tag{6}$$

where $P(Z > z_\beta) = \beta$ with $Z \sim N(0, 1)$. σ_P and σ_S are the standard deviations of a metric associated with the placebo and the atorvastatin groups and δ is the minimum detectable difference. In this paper, the sample sizes were computed that give 90% statistical power (i.e., $\beta = 0.1$) at a significant level of $\alpha = 0.05$.

The stopping criterion of the feature selection algorithm was based on *P*-value obtained for the *t*-test performed based on $\overline{\Delta VWT}_S$. If the selected region is too small, an observer may not have enough information to detect patterns of *VWT-Change* for different treatment groups. Thus, at least 10% of total feature points were selected for this application, and the first check on the *P*-value occurred when 10% of the total feature points had been selected. *P*-values were then obtained at a 1% increment. If *P*-value obtained for *i*% of the total points was higher than the last *P*-value calculated (i.e., for $i-1$% of total points), $i-1$% of total feature points would be selected and the algorithm stops. Too many feature points may prevent an observer from focusing on localized patterns of *VWT-Change* associated with each treatment group. Thus, we limited the number of selected feature points to 50%.

3. Results

3.1. 2D standardized map for example subjects

Figure 5 shows the 3D VWT maps at baseline and follow-up and the 3D *VWT-Change* map and their corresponding 2D standardized maps of an artery in the placebo group. The black-body radiation colour map was used to display VWT and *VWT-Change* maps in this paper as it exhibits perceptual ordering. As a luminance-varying colour map, the black-body radiation colour map facilitates the visualization of small detail and sharp features in a data set (Borland and Taylor 2007). An advantage of this colour map specific to our application is that when *VWT-Change* is displayed, regression, no change and progression are easy to identify as they are respectively represented by dark grey, red and yellow (or white hot at the top of the scale).

Figures 5(a) and (b) show two different views of the 3D VWT maps at baseline. Figures 5(d) and (e) show the views for the 3D VWT maps at three months, and figures 5(g) and (h) show the views for the 3D *VWT-Change* map. The ECA and ICA are respectively on the left and right sides of figures 5(a), (d) and (g), whereas for figures 5(b), (e) and (h), the ECA and ICA are on the right and left sides of the figures respectively. Figures 5(c), (f) and (i) show the 2D standardized map generated for the 3D VWT maps obtained at baseline and follow-up, and the 3D *VWT-Change* map. For this study involving a total of 20 subjects, L_{ICA} and L_{ECA}, as defined in section 2.4.2, were computed to be 21 and 17 mm respectively. The 2D standardized map covers a longitudinal length of 8 mm proximal to the bifurcation and 6 mm distal to the bifurcation. All 2D maps shown in this paper have exactly the same dimensions.

3.2. Average map for each group

Figures 6(a) and (b) show the standardized maps with the average VWT at baseline and follow-up. The average VWT was obtained by taking the mean of the VWT at each point for the ten subjects in the placebo group. Figure 6(a) shows that there were four distinct locations at the CCA and ICA pointed to by the arrows where VWT is higher. These four spots spread out and were associated with higher VWT after three months as appeared in figure 6(b). The *VWT-Change* as shown in figure 6(c) was therefore positive in several large regions in the CCA and ICA, which indicates that VWT of subjects tended to increase if treatment was not provided. Note that this group analysis is only possible with the 2D standardized map developed.

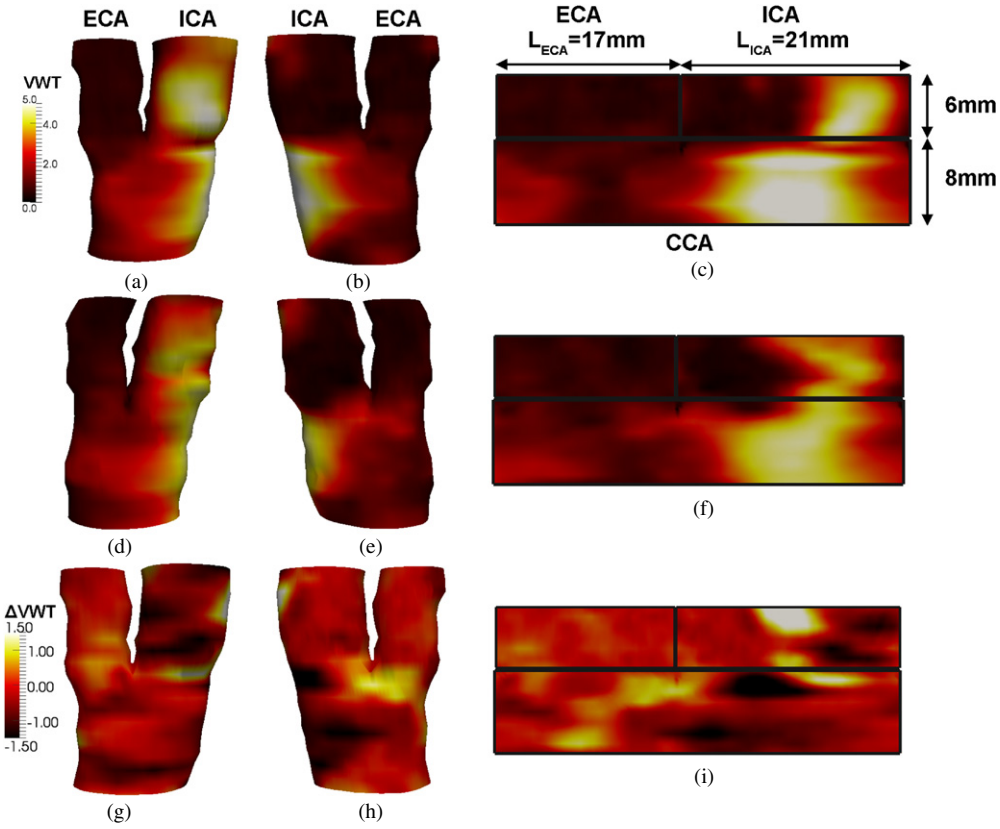

Figure 5. 3D and 2D VWT and *VWT-Change* maps for an example subject. (a) and (b) are two different views of the 3D VWT map at baseline. (c) shows the corresponding 2D VWT map. (d) and (e) are two different views of the 3D VWT map at follow-up, where (f) shows the corresponding 2D VWT map. (g) and (h) show two different views of the 3D *VWT-Change* map with (i) showing the corresponding 2D *VWT-Change* map.

Figures 7(a) and (b) show the standardized maps with the average VWT at baseline and three months later. The average *VWT* was obtained by taking the mean of the VWT at each point for the ten subjects in the atorvastatin group. Figures 7(a) and (b) both show that there is a continuous region at CCA where the vessel wall thickens. This continuous region was cut into two pieces at the right and left end when constructing the 2D standardized map (see arrows). The region shrank during the three months when the subjects were treated by atorvastatin. Figure 7(c) shows the *VWT-Change* map where there is a large region at CCA where regression occurred. There was also an increase of thickness on the left side of figure 7(c). This may due to plaque or vessel wall remodelling in the neighbourhood of large regression.

3.3. Identification of subjects with rapid VWT progression and regression

Figure 8(a) shows the 2D standardized map with $SubjectIndex_P$ (equation (3*a*)) superimposed and regions with $SubjectIndex_P = 5$ shaded in grey. Half the area in the map shown in figure 8(a) was associated with a maximum *VWT-Change* less than or equal to 1 mm and was coloured blue, whereas the rest of the map was associated with a maximum *VWT-Change* greater than 1 mm and superimposed by $SubjectIndex_P$ according to the colour map. 1 mm

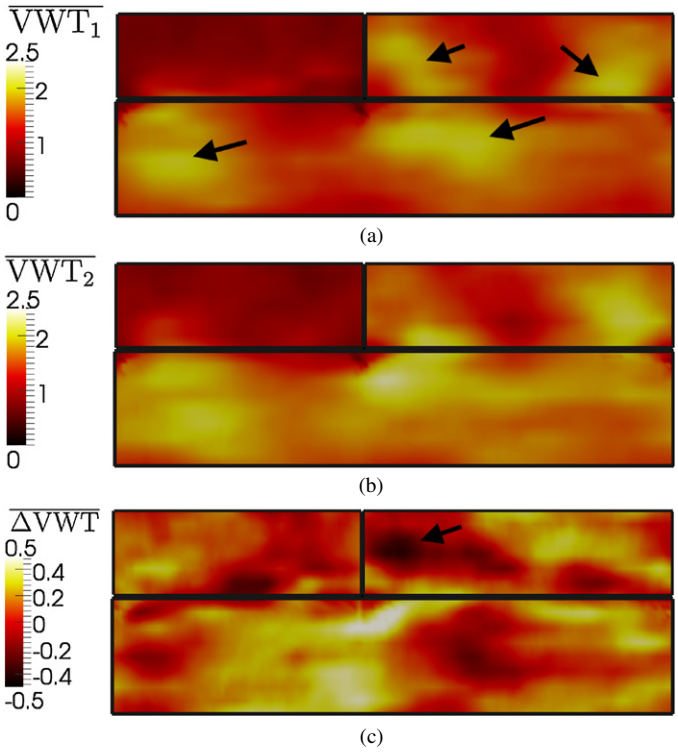

Figure 6. The average 2D VWT and *VWT-Change* maps for the placebo group. (a) The average VWT map at baseline. (b) The average VWT map at follow-up. (c) The average *VWT-Change* map. The four arrows in (a) points to four distinct locations at the CCA and ICA where VWT is higher. The two spots in the CCA and the right spot in ICA spread out after three months as observed in (b), resulting in positive *VWT-Change* in several large regions in CCA and ICA as shown in (c). For the remaining spot in ICA, VWT regressed as pointed to by the arrow in (c).

was chosen to be the threshold to let an observer of figure 8(a) to focus on the progression in the upper 50th percentile. Figure 8(b) shows the 2D ΔVWT map of subject 5 in the placebo group, which had the largest area on the 2D map where the point-by-point VWT progression was maximum among ten subjects in the placebo group. This area was located mainly at the CCA on the left side of the 2D map. Figures 8(c) and (d) show the VWT maps obtained at baseline and follow-up respectively for this subject.

Figure 8(e) shows the 2D map with $SubjectIndex_A$ (equation (3*b*)) superimposed and regions with $SubjectIndex_A = 3$ shaded in grey. The threshold of figure 8(e) was set to 1 mm regression as in equation (3*b*) to facilitate the comparison between the magnitudes of maximum progression and regression shown in figures 8(a) and (e) respectively. Figure 8(e) shows that more than half of the area in the 2D standardized map was coloured blue, indicating less than half of the area in the map was associated with a maximum regression greater than 1 mm in the atorvastatin group. Figure 8(f) shows the VWT map of subject 3 in the atorvastatin group, which had the largest area where the point-by-point VWT regression was maximum among ten atorvastatin subjects. Figures 8(g) and (h) show the VWT maps for this subject obtained at baseline and follow-up respectively. It can be observed that the VWT distribution pattern in figure 8(g) was similar to that in figure 8(h) except that VWT is greatly reduced in regions of CCA displayed in blue colour in the ΔVWT map (figure 8(h)).

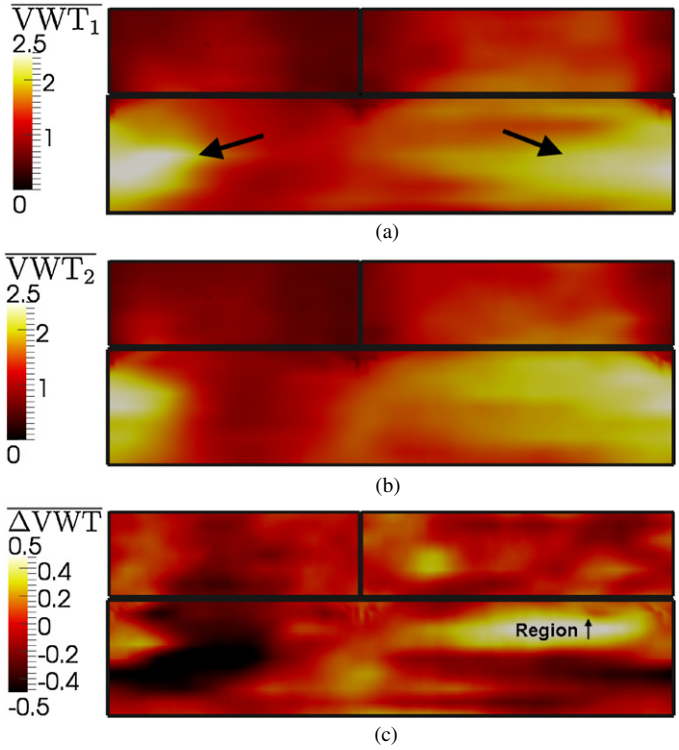

Figure 7. The average 2D VWT and *VWT-Change* maps for the atorvastatin group. (a) The average VWT map at baseline. (b) The average VWT map at follow-up. (c) The average *VWT-Change* map.

3.4. Feature selection results

3.4.1. Relationship between P-value and the number of feature points used. Figure 9 shows the *P*-values associated with the *t*-tests on $\overline{\Delta VWT}_S$ and $\overline{\Delta VWT}_{F_{GD>0}}$ of the placebo and atorvastatin groups against the number of feature points used. It is important to note that the *x*-axis in this graph here represents the number of points (as % of total number of points) selected to put in *S*, the set of all feature points. The set $F_{GD>0}$ has a smaller number of points because only regions where $GD(\Delta VWT)(p_i) > 0$ were included in this set. Figure 9 shows that both *P*-values achieved local minimum when 25% of total points were used as feature points in the calculation of $\overline{\Delta VWT}_S$ and $\overline{\Delta VWT}_{F_{GD>0}}$.

Table 1 shows the means and standard deviations of $\overline{\Delta VWT}_S$ and $\overline{\Delta VWT}_{F_{GD>0}}$ computed for the placebo and atorvastatin groups using different number of feature points. For both metrics, the difference between the means associated with the placebo and atorvastatin groups was larger when a smaller number of feature points were used, while the standard deviations of the means for both groups decreased with the increase of the number of feature points used. As different arteries in a treatment group progress or regress at similar but different locations, a small selected area may not cover the progression/regression locations of all arteries in the same group. *VWT-Change* for some arteries would not be reflected in the mean $\overline{\Delta VWT}_S$ and $\overline{\Delta VWT}_{F_{GD>0}}$ metrics even if changes occurred in the neighbourhood of the selected area. As the selected area becomes larger, it would cover the progression/regression regions of more arteries in a treatment group, reducing the standard deviations of the mean $\overline{\Delta VWT}_S$ and $\overline{\Delta VWT}_{F_{GD>0}}$ metrics. The *t*-test struck a balance between the difference of means and the

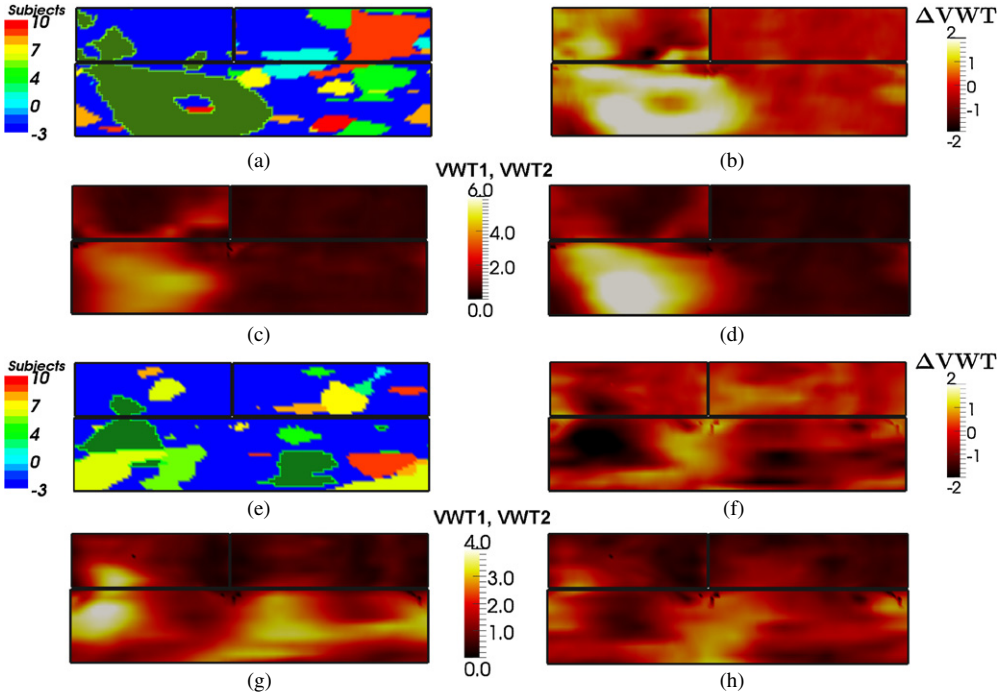

Figure 8. (a) shows the 2D standardized map with $SubjectIndex_P$ (equation (3*a*)) colour-coded and superimposed. This map shows the identification number of the subject with maximum VWT progression among the ten placebo subjects involved in this study if the maximum VWT progression is greater than 1 mm. If the VWT progression is smaller than or equal to 1 mm, -3 is displayed according to equation (3*a*). (b) shows the ΔVWT map of subject 5 in the placebo group, who has the largest area in the 2D map where its point-by-point VWT progression is maximum among ten subjects receiving placebo. (c) and (d) are the VWT maps obtained at baseline and follow-up respectively for subject 5. (e) shows the 2D map with $SubjectIndex_A$ (equation (3*b*)) superimposed. This map shows the identification number of the subject with maximum VWT regression among the ten atorvastatin subjects involved in this study if the maximum VWT regression is greater than 1 mm. If the VWT regression is smaller than or equal to 1 mm, -3 is displayed according to equation (3*b*). (f) shows the ΔVWT map of subject 3 in the atorvastatin group, who has the largest area where its point-by-point VWT regression is maximum among ten subjects receiving atorvastatin. (g) and (h) show the VWT maps obtained at baseline and follow-up respectively for subject 3.

standard deviations of the means, and it is most sensitive for both the $\overline{\Delta VWT}_S$ and $\overline{\Delta VWT}_{F_{GD>0}}$ metrics when the number of feature points selected is 25% of the total number of points in the 2D standardized map. In the rest of the paper, we will present results for the case when the feature selection algorithm selects 25% of the total number of points.

3.4.2. Visualization of feature points on the 2D standardized map. As observed in section 3.2, there are large regions in the average *VWT-Change* map for the placebo group where VWT progressed, which we denote as region I. On the other hand, there are regions in the average *VWT-Change* map for the atorvastatin group where VWT regression occurred, which we denote as region II. Since the aim of the feature selection algorithm is to identify points where the differences between the *VWT-Change* between the placebo and the atorvastatin groups are the most significant, the identified features are expected to include mostly the intersections between region I and region II. In these intersections, the average *VWT-Change*

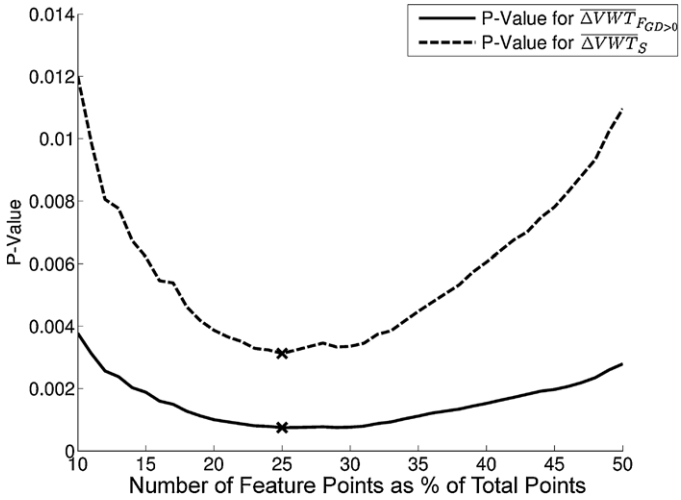

Figure 9. *P*-values associated with the *t*-tests on $\overline{\Delta VWT}_S$ and $\overline{\Delta VWT}_{F_{\mathrm{GD}>0}}$ of the placebo and atorvastatin groups against the number of feature points used. The *P*-values of the two metrics attain their minima when 25% of total points were used as feature points. The minima points are labelled by crosses (×).

Table 1. The mean and standard deviation (in parentheses) of two metrics introduced in section 2.6: $\overline{\Delta VWT}_S$ and $\overline{\Delta VWT}_{F_{\mathrm{GD}>0}}$ computed for the placebo and atorvastatin groups using different number of feature points. *N* denotes the number of feature points used in calculating the two metrics as a percentage of the total number of points in the 2D standardized map. *P*-values associated with *t*-tests based on the two metrics are also tabulated.

	$\overline{\Delta VWT}_S$	$\overline{\Delta VWT}_{F_{\mathrm{GD}>0}}$
	$N = 10\%$	
Placebo group	0.13 (0.34)	0.20 (0.37)
Atorvastatin group	−0.26 (0.27)	−0.34 (0.35)
P	0.012	0.0038
	$N = 20\%$	
Placebo group	0.14 (0.25)	0.20 (0.27)
Atorvastatin group	−0.20 (0.20)	−0.26 (0.25)
P	0.0039	0.0010
	$N = 25\%$	
Placebo group	0.14 (0.24)	0.20 (0.26)
Atorvastatin group	−0.18 (0.17)	−0.24 (0.22)
P	0.0031	7.47×10^{-4}
	$N = 30\%$	
Placebo group	0.15 (0.23)	0.20 (0.25)
Atorvastatin group	−0.15 (0.14)	−0.21 (0.18)
P	0.0034	7.58×10^{-4}

is positive for the placebo group and that for the atorvastatin group is negative, and the difference between these two averages, GD(ΔVWT), is positive (i.e., $F_{\mathrm{GD}>0}$ as defined in section 2.6.1). In presenting the feature selection results, it is important to classify feature points into $F_{\mathrm{GD}>0}$ and $F_{\mathrm{GD}\leqslant 0}$.

Figure 10 shows the results of the feature selection algorithm in which the white and grey regions represent selected feature points. The grey region represents the region $F_{\mathrm{GD}>0}$, and the

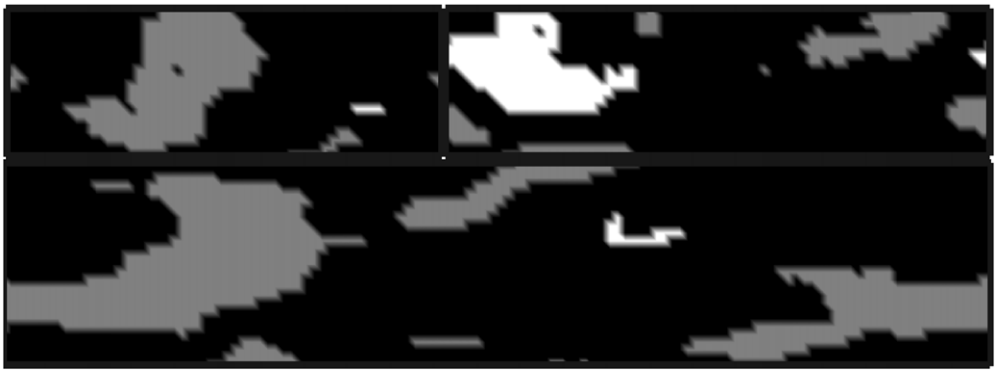

Figure 10. Feature selection result superimposed on the 2D standardized map. Points that were not selected by the feature selection algorithm are coloured in black, whereas white and grey regions represent selected feature points. The grey region represents the region with GD(ΔVWT) (defined in equation (4)) positive, whereas the white region represents the region with GD(ΔVWT) negative.

Table 2. The mean and standard deviation (in parentheses) of three metrics introduced in section 2.6: $\overline{\Delta VWT}$, $\overline{\Delta VWT}_S$ and $\overline{\Delta VWT}_{F_{GD>0}}$ computed for the placebo and atorvastatin groups. For the computation of $\overline{\Delta VWT}_S$ and $\overline{\Delta VWT}_{F_{GD>0}}$, 25% of total points were selected as feature points.

	$\overline{\Delta VWT}$	$\overline{\Delta VWT}_S$	$\overline{\Delta VWT}_{F_{GD>0}}$
Placebo group	0.11 (0.19)	0.14 (0.24)	0.20 (0.26)
Atorvastatin group	−0.03 (0.11)	−0.18 (0.17)	−0.24 (0.22)
P	0.056	0.0031	7.47×10^{-4}

white region represents the region $F_{GD\leqslant 0}$. Feature points are predominantly grey points, which agrees with our expectation. There is also a region on the ICA where the VWT had regressed more in the placebo group than the atorvastatin group, which is mainly due to the regression for the placebo group at that region pointed to by a black arrow in figure 6(c).

3.5. Results of T-tests and sample size estimates

Table 2 shows the means and standard deviations of three metrics described in section 2.6.1. The means of the three metrics computed for the placebo group are all positive, whereas those for the atorvastatin group are all negative. $\overline{\Delta VWT}$ was only slightly negative (−0.03 mm) because the upper right corner region of the CCA (region ↑ in figure 7(c)) is associated with an increase of VWT, possibly due to plaque remodelling in the neighbourhood of large VWT decrease. $\overline{\Delta VWT}$ associated with the placebo and the atorvastatin groups were very close to, but not significantly different in the $\alpha = 0.05$ level ($P = 0.056$).

However, most of the points of region ↑ mentioned above were not selected as feature points since the average *VWT-Change* values computed for the placebo and the atorvastatin groups (figures 6(c) and 7(c)) in this region were not as different as those in other regions of the 2D standardized map (figure 10). As a result, $\overline{\Delta VWT}_S$ is much more negative than $\overline{\Delta VWT}$ for the atorvastatin group (−0.18 mm versus −0.03 mm). The difference between the $\overline{\Delta VWT}_S$ associated with the placebo and the atorvastatin groups were statistically significant ($P = 0.0031$).

Of the 1504 points selected as feature points (25% of total number of points), 1290 points were associated with GD(ΔVWT) > 0. Since only feature points with GD(ΔVWT) > 0 were

Table 3. Sample sizes per group required to show effects of therapy for various effect sizes in a three-month study using the three metrics described in section 2.6. The sample sizes listed below give 90% statistical power at a significance level of 0.05 (two-tailed). The effect sizes are expressed in terms of the percentage of that obtained in the current placebo-controlled clinical study.

Effect size	$\overline{\Delta VWT}$	$\overline{\Delta VWT}_S$	$\overline{\Delta VWT}_{F_{GD>0}}$
100%	24	9	6
75%	43	16	11
50%	97	35	25
25%	390	140	100

involved in the calculation of $\overline{\Delta VWT}_{F_{GD>0}}$, the difference between the $\overline{\Delta VWT}_{F_{GD>0}}$ associated with the placebo and the atorvastatin groups were greater than the difference computed based on the previous two metrics and associated with a smaller P-value ($P = 7.47 \times 10^{-4}$).

Table 3 lists the sample size estimates with effect sizes compared to the current placebo-controlled study. The effect sizes of each metric are expressed in terms of the percentage of that obtained in this study. For the effect size as large as that demonstrated in this study, 24, 9 and 6 subjects per group are required to show a two-tailed difference of $\overline{\Delta VWT}$, $\overline{\Delta VWT}_S$ and $\overline{\Delta VWT}_{F_{GD>0}}$ respectively with a power of 90% and a significant level of 0.05. The required sample size would be a much more important issue if the effect size was smaller. For example, if the effect size for a trial was 25% of the current trial, it would require 390 subjects to demonstrate a difference of $\overline{\Delta VWT}$ at the selected power and level of significance. The number of subjects required would be reduced by at least a half if the feature selection algorithm was applied ($n = 140$ for $\overline{\Delta VWT}_S$ and $n = 100$ for $\overline{\Delta VWT}_{F_{GD>0}}$).

4. Discussion and conclusion

Management of carotid atherosclerosis through lifestyle changes and medical therapy has the potential to reduce the risk of vascular events by 75% to 80% (Spence 2007). In addition to these conventional treatments, many new molecular therapies and phenotypic therapeutic targets have been identified and developed (Nabel 1995, Rissanen and Ylä-Herttuala 2007, Flynn *et al* 2011). As new therapies are continually being developed, an equally important requirement is the development of sensitive, cost-effective and non-invasive measurement tools and biomarkers that can be used to assess the efficacy of various treatment strategies. The ultimate goal of this paper is to develop such a biomarker.

The biomarker we proposed in this paper is based on the local distribution of *VWT-Change* associated with different treatment groups. In order to make *VWT-Change* distribution of different subjects comparable, the first step was to develop a 2D standardized template onto which all carotid arteries involved in the study are mapped. Since the point-by-point *VWT-Change* values of all arteries were mapped to the standardized 2D map, an average map of *VWT-Change* for each treatment group can be generated. The average *VWT-Change* map for the placebo group (figure 6(c)) and the atorvastatin group (figure 7(c)) can be displayed and compared. This groupwise comparison was only possible with the development of the 2D standardized map.

The 2D standardized map has also allowed for the identification of subjects with rapid plaque progression, which is a factor for elevated stroke risk (Spence *et al* 2002, Hirano *et al* 2011). We demonstrated the use of the 2D standardized map to identify regions in which an artery exhibited maximum point-by-point VWT progression among the ten arteries in the placebo group. Although only the subjects with maximum progression and regression were

shown in figure 8, each subject j in the placebo group is associated with an area where its point-by-point VWT progression is maximum on the 2D standardized map (i.e., the area with the subject number, j, superimposed in figure 8(a)). Subjects can be ranked according to this area and this ranking can be taken into consideration when assessing relative risk of vascular events. Similarly, each subject in the atorvastatin group can be ranked according to its associated area in figure 8(e).

One limit of this pilot study is that it only involved a small number of subjects. Larger clinical trials should be designed and carried out in the future to address two important issues: (a) Does subject j's relative risk of vascular events depend on the area on the 2D map where this subject has the maximum point-by-point VWT progression? (b) Does the risk of vascular outcomes depend on where the VWT progression is located? For example, according to figure 8(a), subject 5 had maximum VWT progression mainly at the CCA, whereas subject 9 had maximum VWT progression mainly at the ICA. Who would be more prone to have vascular events? The relative risks associated with the two arteries should be normalized by the area discussed in (a) in order to make a fair comparison between them. In a similar way, subjects with rapid response to therapies can be identified as displayed in figure 8(e). Similar to the case for rapid VWT progression, a larger trial would be required to establish whether the relative risk of vascular events is significantly lower for a subject with large area on the 2D map where its point-by-point VWT regression is maximum.

Another goal of this paper is to develop a more sensitive test to quantify the effects of various treatment strategies based on the spatio-temporal information of VWT provided by the 2D standardized map. Our approach is to apply a feature selection algorithm as a quantitative and objective method to identify regions on the 2D map where subjects in the placebo group and the atorvastatin group exhibit greater difference in *VWT-Change*. A mutual-information-based feature selection technique using sequential forward searching strategy was employed. This method is classified as one of the filter methods in feature selection literature (Liu and Yu 2005), in which the feature selection criterion (e.g., mutual information) is independent of any classification model. A filter method, instead of a wrapper method, in which the evaluation criterion depends on the classification model, is suitable for this study because our goal was not on classifying the carotid artery to the atorvastatin or placebo groups based on the *VWT-Change* distribution. We already knew which treatment group each artery belongs to (i.e., the classification label in machine learning language), and with this information, we attempted to find a subset of points that correlate to the greatest extent with the classification label. Having selected that we would use a filter method, the next step was to decide which feature selection criterion should be used. Mutual information was chosen as it is less sensitive to noise than other statistics (Narendra and Fukunaga 1977, Liu *et al* 1998). The most apparent characteristic of the carotid data set in this study is that the ratio between the number of features (6016 points) and the number of subjects (20 in total) was very large. The mutual-information estimation algorithm proposed in Chow and Huang (2005) using Parzen window was tailored for this high-dimensional small data point problem. The algorithm we employed adopted the sequential forward searching strategy, which is computationally very efficient (Liu and Yu 2005). Since there were so many feature points in the standardized carotid map, computational efficiency was a very important consideration. Other searching technique such as genetic algorithm (GA) (Yang and Honavar 1998), while more probable to achieve optimality, would definitely be less computationally efficient. While our technique is more computationally efficient, the feature subset obtained may not maximize mutual information in the optimal sense. Thus, the feature selection results generated must be carefully evaluated (which is the focus of the discussion in the next paragraph). Another reason that we decided against using GA was that it is not suitable for a study with a relatively small sample size. One of the problems is that it is not

Table 4. Sample sizes per group required to detect a 25% effect size in a six-month study with 90% power at a significance level of 0.05 (two-tailed). The progression on placebo and regression on active treatment are assumed to be linear. Sources of the data used in the calculation: Bots *et al* (2003) for IMT, Hackam *et al* (2000) for plaque area and Krasinski *et al* (2009) for VWV.

Biomarkers	*N* per group
IMT	17465
Plaque area	2260
VWV	133
$\overline{\Delta VWT}$	97
$\overline{\Delta VWT}_S$	35
$\overline{\Delta VWT}_{F_{GD>0}}$	25

apparent as to how GA should be initialized in order for it to converge to a reasonable solution given the small sample size.

A performance metric is required for feature selection evaluation. Classification error rate is a commonly used evaluation metric, which is typically obtained for the full feature set and the selected subset and then compared (Liu and Yu 2005). For our study, we applied a more biologically relevant metric to evaluate the quality of feature selected: for each artery, we first calculated $\overline{\Delta VWT}$ (equation (5*a*)), which is the average *VWT-Change* computed over the whole artery, and $\overline{\Delta VWT}_S$ and $\overline{\Delta VWT}_{F_{GD>0}}$ (equations (5*b*) and (5*c*)), which are averages of *VWT-Change* computed over selected regions on the artery. *T*-tests were performed to test the statistical significance between the placebo and atorvastatin groups on three averages of *VWT-Change* (i.e., equations (5*a*)–(5*c*)). Each *t*-test is associated with a *P*-value, which reflects the sensitivity of the three averages of *VWT-Change*. We demonstrated that $\overline{\Delta \mathrm{VWT}}_S$ and $\overline{\Delta \mathrm{VWT}}_{F_{GD>0}}$ were more sensitive than $\overline{\Delta VWT}$ (table 2), and therefore showed that the feature selection results we obtained were sufficiently accurate for our application.

We computed the sample sizes required to show statistical significance between the atorvastatin and the placebo group using the three averages of *VWT-Change* . For an effect size of 25% of the current trial, the sample size required to show statistical significance between the placebo and atorvastatin groups based on $\overline{\Delta VWT}$ with a power of 90% and a significance level of 0.05 in a six-month study is 97 per group. For the same effect size, power and significance level, the sample size required for the *VWV* study (Krasinski *et al* 2009) to show a statistically significant difference between the placebo and atorvastatin groups was 133 per group, which is comparable to the sample size obtained for $\overline{\Delta VWT}$. This is not unexpected because $\overline{\Delta VWT}$ is approximately equal to the *VWV* scaled by 3D surface area. The sample sizes required for $\overline{\Delta VWT}_S$ and $\overline{\Delta VWT}_{F_{GD>0}}$ to detect the same effect size at the same power and significance level were reduced to 35 and 25 respectively, showing evidences to support our hypothesis that statistical tests performed on regions chosen by the feature selection algorithm require fewer subjects per group to achieve statistical significance. The subjects involved in this study had a large plaque burden and the dosage of atorvastatin administered to subjects assigned to the atorvastatin group is high. The effect size of most clinical trials would likely to be smaller than this trial. In this situation, the sample size reduction by using $\overline{\Delta VWT}_S$ and $\overline{\Delta VWT}_{F_{GD>0}}$ instead of $\overline{\Delta VWT}$ would be more significant. Table 3 shows that if the effect size for a trial was 25% of the current trial, the sample size required to achieve statistically significant difference in a three-month study would be reduced from 390/group if $\overline{\Delta VWT}$ was used to 140 and 100/group if $\overline{\Delta VWT}_S$ and $\overline{\Delta VWT}_{F_{GD>0}}$ were used, respectively.

To put the sample sizes required in the metrics introduced in this paper in context, the sample sizes required to show effects of therapy using different ultrasound phenotypes were calculated and shown in table 4. In the calculation, the duration of the studies was all set

to be six months. The progression and regression of the placebo and the group receiving treatments respectively are assumed to be linear. Thus, linear interpolation/extrapolation was used to estimate the progression on placebo and the regression on active treatment. Sources of the data used in the calculations are from Bots *et al* (2003) for IMT, Hackam *et al* (2000) for plaque area and Krasinski *et al* (2009) for VWV. Since plaque area increases 2.4 times faster than plaque thickness (Barnett *et al* 1997), it is not surprising that sample sizes required to show effects of therapy for plaque area are much smaller than IMT. In addition, plaque does not only grow along the artery, but also progresses circumferentially. Thus, vessel wall volume (VWV) measured from 3D ultrasound is much more sensitive than IMT and plaque area measurements, requiring a much smaller sample size to detect effects of treatments. In this paper, we combined the use of the standardized 2D *VWT-Change* map and a mutual-information-based feature selection technique in quantifying the difference between VWT progression of subjects on placebo and on atorvastatin. Table 4 provided evidences to support our hypothesis that metrics accounting for *VWT-Change* only in regions where the *VWT-Change* distribution patterns exhibited by the placebo and atorvastatin groups are significantly different (as determined by the feature selection algorithm) are much more sensitive and leads to a further reduction of the sample size requirement comparing to global 1D (IMT), 2D (plaque area) and 3D (VWV) measurements. It is important to note that feature selection analysis was possible only because corresponding regions of carotid arteries in different treatment groups were able to be mapped to a standardized map using the proposed 2D mapping technique. The increase of cost-effectiveness introduced by the proposed technique would allow many more smaller trials to be performed by investigators developing new treatment options.

Acknowledgments

The authors thank Dr Aaron Fenster for providing the 3D ultrasound images and manually segmented contours for this analysis. This study described in this paper is supported by the National Natural Science Foundation of China (grant no. 81201149) and City University of Hong Kong Strategic Research grant no. 7002871 awarded to Dr Bernard Chiu.

References

Ainsworth C D, Blake C C, Tamayo A, Beletsky V, Fenster A and Spence J D 2005 3D ultrasound measurement of change in carotid plaque volume: a tool for rapid evaluation of new therapies *Stroke* **36** 1904–9

Barnett P A, Spence J D, Manuck S B and Jennings J R 1997 Psychological stress and the progression of carotid artery disease *J. Hypertens.* **15** 49–55

Bartroli A V, Wegenkittl R, Konig A and Groller E 2001 Nonlinear virtual colon unfolding *VIS'01: Proc. Conf. on Visualization* (Washington, DC: IEEE Computer Society) pp 411–20

Battiti R 1994 Using mutual information for selecting features in supervised neural net learning *IEEE Trans. Neural Netw.* **5** 537–50

Borland D and Taylor M R 2007 Rainbow color map (still) considered harmful *IEEE Comput. Graph. Appl.* **27** 14–17

Bots M L, Evans G W, Riley W A and Grobbee D E 2003 Carotid intima-media thickness measurements in intervention studies: design options, progression rates, and sample size considerations: a point of view *Stroke* **34** 2985–94

Browne J E, Watson A J, Gibson N M, Dudley N J and Elliott A T 2004 Objective measurements of image quality *Ultrasound Med. Biol.* **30** 229–37

Chiu B, Beletsky V, Spence J D, Parraga G and Fenster A 2009 Analysis of carotid lumen surface morphology using three-dimensional ultrasound imaging *Phys. Med. Biol.* **54** 1149–67

Chiu B, Egger M, Spence J D, Parraga G and Fenster A 2008a Area-preserving flattening maps of 3D ultrasound carotid arteries images *Med. Image Anal.* **12** 676–88

Chiu B, Egger M, Spence J D, Parraga G and Fenster A 2008b Quantification of carotid vessel wall and plaque thickness change using 3D ultrasound images *Med. Phys.* **35** 3691–710

Chiu B, Shamdasani V, Entrekin R, Yuan C and Kerwin W S 2012 Characterization of carotid plaques on 3-dimensional ultrasound imaging by registration with multicontrast magnetic resonance imaging *J. Ultrasound Med.* **31** 1567–80 PMID: 23011620

Chiu B, Ukwatta E, Shavakh S and Fenster A 2013 Quantification and visualization of carotid segmentation accuracy and precision using a 2D standardized carotid map *Phys. Med. Biol.* **58** 3671–703

Chow T W S and Huang D 2005 Estimating optimal feature subsets using efficient estimation of high-dimensional mutual information *IEEE Trans. Neural Netw.* **16** 213–24

ECST Collaborative Group 1995 Risk of stroke in the distribution of an asymptomatic carotid artery *Lancet* **345** 209–12

Egger M, Chiu B, Spence J D, Fenster A and Parraga G 2008 Mapping spatial and temporal changes in carotid atherosclerosis from three-dimensional ultrasound images *Ultrasound Med. Biol.* **34** 64–72

Egger M, Spence J D, Fenster A and Parraga G 2007 Validation of 3D ultrasound vessel wall volume: an imaging phenotype of carotid atherosclerosis *Ultrasound Med. Biol.* **33** 905–14

Eicke B M, von Lorentz J and Paulus W 1995 Embolus detection in different degrees of carotid disease *Neurol. Res.* **17** 181–4 PMID: 7643973

Fenster A, Downey D B and Cardinal H N 2001 Three-dimensional ultrasound imaging *Phys. Med. Biol.* **46** R67–99

Flynn R, Qian K, Tang C, Dronadula N, Buckler J M, Jiang B, Wen S, Dichek H L and Dichek D A 2011 Expression of apolipoprotein A-I in rabbit carotid endothelium protects against atherosclerosis *Mol. Ther.* **19** 1833–41

Golledge J, Greenhalgh R M and Davies A H 2000 The symptomatic carotid plaque *Stroke* **31** 774–81

Gorelick P B 1994 Stroke prevention An opportunity for efficient utilization of health care resources during the coming decade *Stroke* **25** 220–4

Hackam D G, Peterson J C and Spence J D 2000 What level of plasma homocyst(e)ine should be treated? Effects of vitamin therapy on progression of carotid atherosclerosis in patients with homocyst(e)ine levels above and below 14 micromol/l *Am. J. Hypertens.* **13** 105–10

Haker S, Angenent S, Tannenbaum A and Kikinis R 2000 Nondistorting flattening maps and the 3-D visualization of colon ct images *IEEE Trans. Med. Imaging* **19** 665–70

He J *et al* 2005 Major causes of death among men and women in china *New Engl. J. Med.* **353** 1124–34

Hirano M *et al* 2011 Short-term progression of maximum intima-media thickness of carotid plaque is associated with future coronary events in patients with coronary artery disease *Atherosclerosis* **215** 507–12

Krasinski A, Chiu B, Spence J D, Fenster A and Parraga G 2009 Three-dimensional ultrasound quantification of intensive statin treatment of carotid atherosclerosis *Ultrasound Med. Biol.* **35** 1763–72

Landry A, Spence J D and Fenster A 2004 Measurement of carotid plaque volume by 3-dimensional ultrasound *Stroke* **35** 864–9

Liu H, Motoda H and Dash M 1998 A monotonic measure for optimal feature selection *Machine Learning: ECML-98: 10th European Conf. on Machine Learning (Chemnitz, Germany, 21–23 April)* (Berlin: Springer) pp 101–6

Liu H and Yu L 2005 Toward integrating feature selection algorithms for classification and clustering *IEEE Trans. Knowl. Data Eng.* **17** 491–502

Lloyd-Jones D *et al* 2010 Heart disease and stroke statistics–2010 update: a report from the American Heart Association *Circulation* **121** e46–215

Nabel E G 1995 Gene therapy for cardiovascular disease *Circulation* **91** 541–8

Narendra P M and Fukunaga K 1977 A branch and bound algorithm for feature subset selection *IEEE Trans. Comput.* **100** 917–22

NASCET Steering Committee 1991 North American symptomatic carotid endarterectomy trial Methods, patient characteristics, and progress *Stroke* **22** 711–20

O'Leary D H and Polak J F 2002 Intima-media thickness: a tool for atherosclerosis imaging and event prediction *Am. J. Cardiol.* **90** 18L–21L

Pollex R L, Spence J D, House A A, Fenster A, Hanley A J, Zinman B, Harris S B and Hegele R A 2005 A comparison of ultrasound measurements to assess carotid atherosclerosis development in subjects with and without type 2 diabetes *Cardiovasc. Ultrasound* **3** 15

Rissanen T T and Yl-Herttuala S 2007 Current status of cardiovascular gene therapy *Mol. Ther.* **15** 1233–47

Spence J D 2007 Intensive management of risk factors for accelerated atherosclerosis: the role of multiple interventions *Curr. Neurol. Neurosci. Rep.* **7** 42–48

Spence J D, Eliasziw M, DiCicco M, Hackam D G, Galil R and Lohmann T 2002 Carotid plaque area: a tool for targeting and evaluating vascular preventive therapy *Stroke* **33** 2916–22

Ukwatta E, Awad J, Ward A D, Buchanan D, Samarabandu J, Parraga G and Fenster A 2011 Three-dimensional ultrasound of carotid atherosclerosis: semiautomated segmentation using a level set-based method *Med. Phys.* **38** 2479–93

Yang J and Honavar V 1998 Feature subset selection using a genetic algorithm *IEEE Int. Syst. Appl.* **13** 44–49

Zhu L, Haker S and Tannenbaum A 2005 Flattening maps for the visualization of multibranched vessels *IEEE Trans. Med. Imaging* **24** 191–8